Volume 9
Number 3
21 January 2021
Pages 1279–1870

Journal of Materials Chemistry A

Materials for energy and sustainability

rsc.li/materials-a

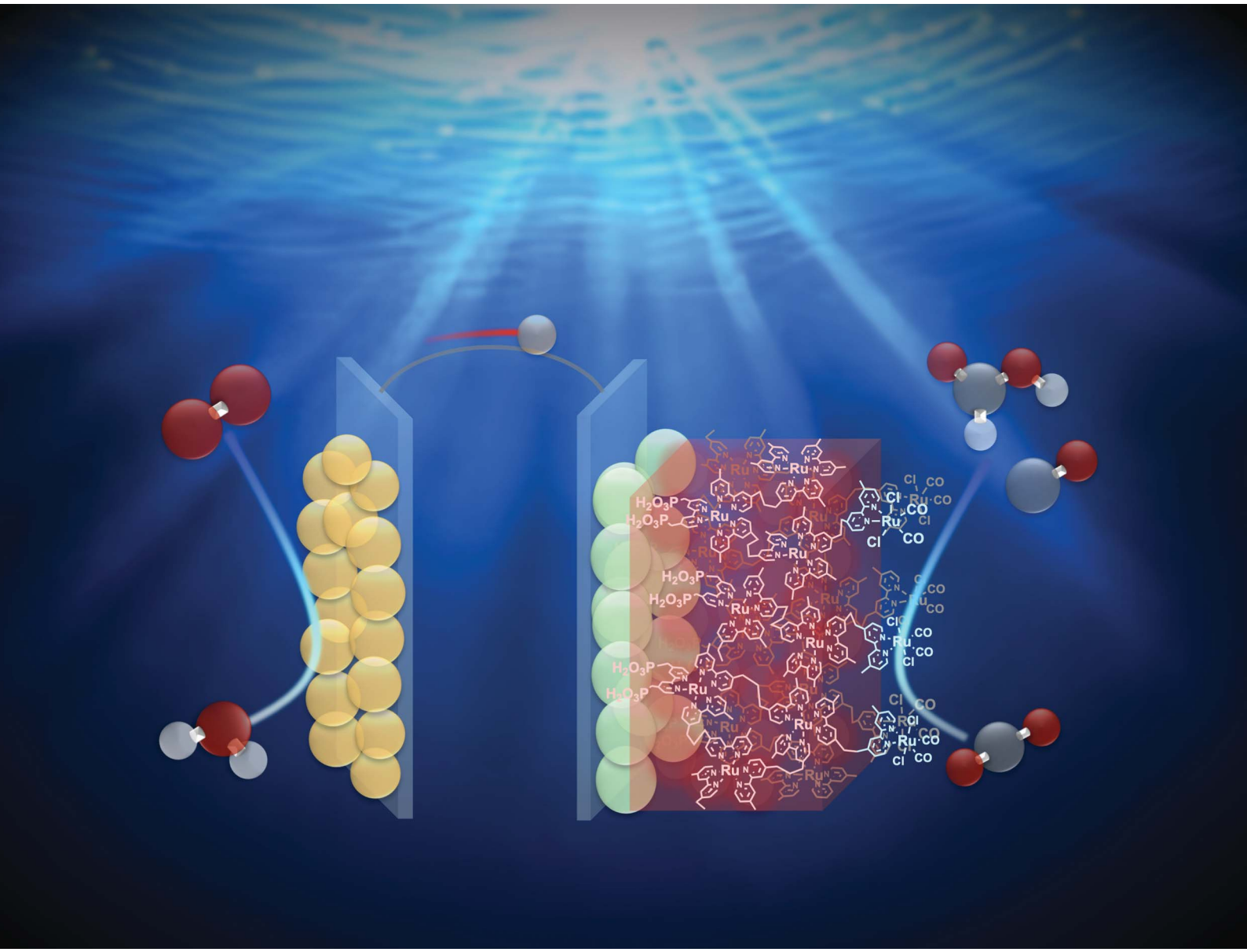

ISSN 2050-7488

ROYAL SOCIETY OF CHEMISTRY

PAPER

Osamu Ishitani *et al.*

Durable photoelectrochemical CO_2 reduction with water oxidation using a visible-light driven molecular photocathode

Journal of Materials Chemistry A

ROYAL SOCIETY OF CHEMISTRY

PAPER

View Article Online
View Journal | View Issue

Cite this: J. Mater. Chem. A, 2021, 9, 1517

Durable photoelectrochemical CO_2 reduction with water oxidation using a visible-light driven molecular photocathode†

Ryutaro Kamata,[a] Hiromu Kumagai, ‡[a] Yasuomi Yamazaki, §[a] Masanobu Higashi,¶[b] Ryu Abe [b] and Osamu Ishitani *[a]

Photocatalytic reduction of CO_2 using water as a reductant and visible light as the energy source is an important target in artificial photosynthesis. In this study, we report a highly stable photoelectrochemical CO_2 reduction involving a new molecular photocathode comprising a NiO electrode and polymerized complexes of the Ru(II) photosensitizer and Ru(II) catalyst (NiO/**PRu**-*poly*-**Ru**-**RuCAT1**). CO and HCOOH were stably and selectively produced for over 100 h under visible light irradiation and a low bias. The turnover number of CO_2 reduction products exceeded 1200, which represents the highest durability reported for photoelectrochemical reactions using molecular photocathodes. Moreover, a connected system of the NiO/**PRu**-*poly*-**Ru**-**RuCAT1** molecular photocathode and a CoO_x/$BiVO_4$ photoanode suitable for water oxidation facilitated stable CO_2 reduction with water as an electron donor and visible light as the energy source, with no bias for over 24 h. An energy conversion efficiency of 1.7×10^{-2}% was obtained, which is the highest value reported for visible light driven systems utilizing a molecular photocatalyst for CO_2 reduction with water as the reductant.

Received 28th July 2020
Accepted 15th September 2020

DOI: 10.1039/d0ta07351b

rsc.li/materials-a

Introduction

Artificial photosynthesis is an attractive research field because of its potential to resolve three serious problems facing mankind; global warming, shortage of energy resources, and carbon resource scarcity. Therefore, photocatalytic reduction of CO_2 with water as a reductant and visible light as the energy source is one of the most important aims in artificial photosynthesis research. Few systems achieve this reaction without employing expensive tandem-type solar cells, with the carbon and electron sources clearly determined. Morikawa and his co-workers reported systems which consisted of two types of semiconductor photoelectrodes, one p-type InP semiconductor photocathode with a Ru(II) carbonyl complex as a catalyst for CO_2 reduction and another TiO_2 photoanode.[1] The efficiency of this type of photoelectrochemical cell for CO_2 reduction has been improved, such as using a coupled system of a reduced $SrTiO_3$ photoanode for water oxidation and a TiO_2/N,Zn-Fe_2O_3/Cr_2O_3 photocathode with a Ru(II)-complex as a catalyst for CO_2 reduction.[2] However, the photoanode of these systems cannot absorb visible light. Recently, Morikawa, Kudo, and colleagues also reported a mixed system of two types of semiconductor particles, *i.e.*, $(CuGa)_{1-x}Zn_{2x}S_2$ and $BiVO_4$. In this system, the Ru(II) complex was again used as the catalyst for CO_2 reduction.[3] The reported systems exhibit a low selectivity of CO_2 reduction against H_2 evolution and insufficient durability. It is again emphasized that, in these systems, light absorbers are the semiconductor materials, and the Ru(II) complex works only as the catalyst.

We recently reported novel types of molecular photocathodes consisting of supramolecular photocatalysts with two types of metal complexes as redox photosensitizer (PS) and catalyst (CAT) units in one molecule and a p-type semiconductor electrode like NiO and $CuGaO_2$ which has no or weak absorption in the visible region.[4–7] These molecular photocathodes can reduce CO_2 under visible light irradiation and a relatively low-applied potential. The photocatalytic reactions were initiated by the excitation of only the PS unit of the supramolecular photocatalyst and not by excitation of the semiconductor material. These new molecular photocathodes should be advantageous over the systems coupling two

[a]Department of Chemistry, School of Science, Tokyo Institute of Technology, O-okayama 2-12-1-NE-1, Meguro-ku, Tokyo 152-8550, Japan. E-mail: ishitani@chem.titech.ac.jp

[b]Department of Energy and Hydrocarbon Chemistry, Graduate School of Engineering, Kyoto University, Katsura, Nishikyo-ku, Kyoto 615-8510, Japan

† Electronic supplementary information (ESI) available: UV-vis spectra, time courses of photocurrent at various potentials, FT-IR spectra of NiO/**PRu**-*poly*-**Ru**-**RuCAT2**, and the SEM image. See DOI: 10.1039/d0ta07351b

‡ Present address: Institute of Multidisciplinary Research for Advanced Materials, Tohoku University, 2-1-1 Katahira, Aoba-ku, Sendai, Miyagi 980-8577, Japan.

§ Present address: Department of Materials and Life Science, Graduate School of Science and Engineering, Seikei University, 3-3-1 Kichijoji-kitamachi, Musashino-shi, Tokyo 180-8633, Japan.

¶ Present address: The OCU Advanced Research Institute for Natural Science and Technology, Osaka City University, 3-3-138 Sugimoto, Sumiyoshiku, Osaka City, Osaka, 558-8585, Japan.

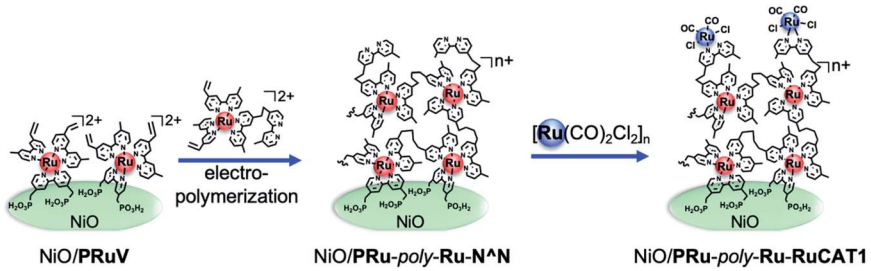

Scheme 1 Preparation scheme for NiO/PRu-*poly*-Ru-RuCAT1.

semiconductor materials as light absorbers and a mononuclear metal complex only as a catalyst. We can easily change the absorption wavelength and the ability of the photocathode by changing the PS unit of the supramolecular photocatalysts on the electrode. Since intramolecular electron transfer rapidly proceeds from the reduced PS unit to the CAT unit,[8,9] the electrons supplied from the semiconductor electrode to the PS unit can be efficiently and rapidly transferred to the CAT unit. Since the distance between the CAT unit of the supramolecular photocatalyst and the electrode is larger compared to the photocathode where the mononuclear metal complex as the CAT was directly attached on the electrode, the back-electron-transfer from the reduced CAT to the electrode, which lowers the efficiency of the photocathodic reaction, can be suppressed. Moreover, since the excited states of the PS units such as the Ru(II) trisdiimine complexes have stronger oxidation power compared to those of p-type semiconductors such as InP, visible-driven photoanodes such as TaON and $BiVO_4$ can be potentially coupled as photoanodes for water oxidation.

We reported photoelectrochemical cells comprising this new type of molecular photocathode and a visible-light driven n-type semiconductor photoanode for H_2O oxidation in CO_2 reduction *i.e.* water serves as an electron donor and visible light as the energy source.[5,6] These are the sole examples of using a supramolecular photocatalyst for CO_2 reduction with water as a reductant and visible light as energy. However, the reaction durability of these molecular photocathodes is still insufficient; the reaction rate of the system significantly decreases within a few hours. This low stability is primarily attributed to the desorption of the supramolecular photocatalyst from the semiconductor electrode during the photoreaction. Notably, such desorption of the metal complex has been frequently highlighted as an essential problem in the metal complex–semiconductor hybrids,[10–13] owing to insufficient adsorption by the anchoring groups such as phosphonic and carboxylic acids in water solutions, especially during photoredox reactions.

To solve this problem, several methods such as stabilization by polymerization of a metal complex,[1,7,14–20] formation of an overlayer by atomic layer deposition,[21–23] and amide coupling using surface-decorated silatrane anchoring groups[24] are proposed. For example, molecular photocathodes prepared through adsorption of Ru(II) PS and Re(I) CAT units by electropolymerization have been reported by our and Meyer's groups.[7,20] These photocathodes facilitate relatively stable photoreactions compared to those using only anchoring groups. Nevertheless, the improved stability remains limited; their photocurrent is maintained for several hours but decreases over longer irradiation owing to the splitting of the Re–C bonds, which were made in the side reaction during the electropolymerization,[7] causing the metal complexes to be soluble in the reaction solution. So far, no attempt has increased the reaction time beyond 15 h, and the turnover numbers (TON) for CO_2 reduction were usually less than 100.[5–7,20] Therefore, an optimized design is required for the synthesis of the molecular photocathode for CO_2 reduction, to improve durability.

Herein, we report a highly durable and efficient photoelectrochemical CO_2 reduction using a novel molecular photocathode (NiO/**PRu**-*poly*-**Ru-RuCAT1**) prepared by a new three-step procedure (Scheme 1), which does not produce by-products of the metal–carbon bonds. First, the Ru trisdiimine-type photosensitizer complex (**PRuV**, Fig. 1), containing both methyl phosphonic acid groups and vinyl groups on the diimine ligands, was adsorbed by methyl phosphonic acid groups on a NiO electrode. Another Ru mononuclear complex possessing diimine ligands with a vinyl group and a non-coordinated diimine ligand (**VRu-N^N**, Fig. 1) was connected by electropolymerization of the vinyl groups. These procedures induced the rigid attachment of the polymerized Ru redox photosensitizer complexes with a non-coordinated diimine ligand onto the NiO electrode and increased the amount of the attached Ru photosensitizer units. Finally, a Ru catalyst unit was introduced into the non-coordinated diimine ligand, forming $[(N^N)_2Ru(bpyC_2bpy)Ru(CO)_2Cl_2]^{2+}$-type complexes (N^N = diimine ligand, $bpyC_2bpy$ = 1,2-bis(4′-methyl-[2,2′-bipyridine]-4-yl) ethane) on the electrode, which were reported as durable supramolecular photocatalysts for CO_2 reduction in homogeneous solutions[25] and hybrid systems with various

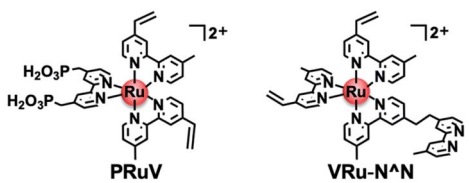

Fig. 1 Chemical structures of the metal complexes used as monomers in this report.

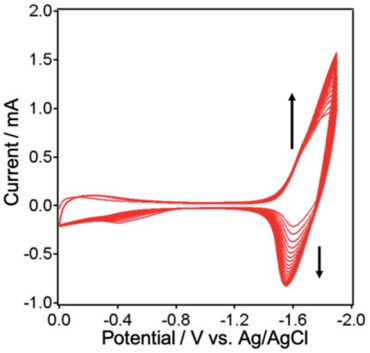

Fig. 2 Cyclic voltammogram during electropolymerization of **VRu-N^N** on NiO/**PRuV** (electrode area: 2.5 cm^2) in an Ar saturated MeCN solution containing **VRu-N^N** (0.5 mM) and Et_4NBF_4 (0.1 M) as an electrolyte. The potential was repeatedly applied (20 times) between 0 to −1.9 V at a scan rate of 100 mV s^{-1}.

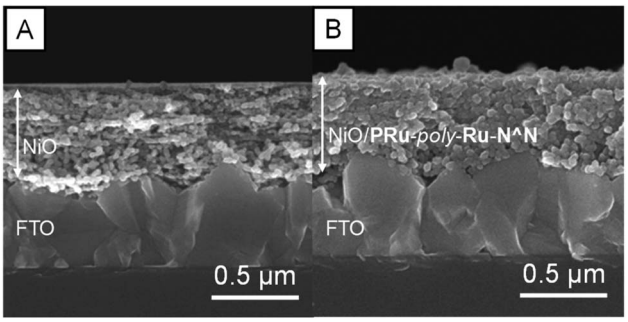

Fig. 3 Cross-sectional scanning electron microscopy (SEM) images of (A) the NiO electrode and (B) NiO/**PRu**-poly-**Ru-N^N**.

semiconductor particles.[10–13] This three-step procedure prevented structural changes of the catalyst unit during the electropolymerization. The NiO/**PRu-*poly*-Ru-RuCAT1** molecular photocathode displayed excellent stability for the photoelectrochemical CO_2 reduction with an applied bias at $E = -0.7$ V *vs.* Ag/AgCl for longer than 100 h. This is the most stable molecular photocathode up to now. In addition, combining this molecular photocathode with a suitable semiconductor photoanode yielded stable photocatalytic CO_2 reduction using water as an electron donor and visible light as an energy source, without bias for over 24 h.

Results and discussion

Preparation of NiO/PRu-*poly*-Ru-RuCAT1

NiO electrodes were prepared by coating a NiO film on fluorine doped tin oxide (FTO) electrodes (active area: 2.5 cm^2).[4] NiO/**PRuV** was prepared by a simple adsorption method *via* dipping the NiO electrode into an MeCN solution containing **PRuV** overnight. This was used as a working electrode for electropolymerization of the Ru complexes, using a three-electrode system in an Ar-purged MeCN solution containing **VRu-N^N** and a tetraethylammonium tetrafluoroborate (Et_4NBF_4) supporting electrolyte. The potential was scanned between 0 V and −1.9 V (*vs.* $Ag/AgNO_3$) at a scan rate of 100 mV s^{-1} for 20 cycles during the polymerization. Current corresponding to redox reactions of the Ru(II) photosensitizer units was evident between −1.3 V and −1.9 V, increasing with the number of sweep cycles (Fig. 2). These results suggest that **VRu-N^N** polymerized and adsorbed on the electrode, producing NiO/**PRu-*poly*-Ru-N^N**.[7] Scanning electron microscopy (SEM) images of NiO and NiO/**PRu-*poly*-Ru-N^N** reveal that the Ru complex polymer formed on the surface and inside the layer among the NiO particles (Fig. 3). Fig. 4 shows the results from time-of-flight secondary ion mass spectrometry (TOF-SIMS), demonstrating the distribution of elements in the depth direction for specimens of NiO, NiO/**PRuV**, and NiO/**PRu-*poly*-Ru-N^N**. The sputter times on the horizontal axis correspond to the cross-sectional components in the depth direction of the electrode. The relatively higher intensity of Ru^+ species throughout the entire range was confirmed for NiO/**PRuV** and NiO/**PRu-*poly*-Ru-N^N**, whereas the polymer prepared by the previously reported synthesis method showed the non-uniform distribution of Ru near the surface of the NiO layer of the electrode.[7] This clearly indicates that the Ru complex penetrates the NiO film layer by adsorbing **PRuV** and following the electropolymerization of **VRu-N^N**.

The UV-vis absorption spectrum of NiO/**PRu-*poly*-Ru-N^N** shows a characteristic absorption maximum at around 464 nm,

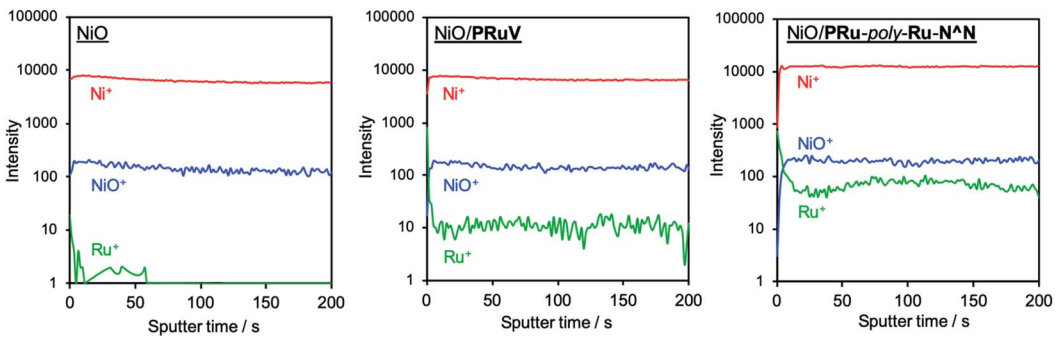

Fig. 4 Time-of-flight secondary ion mass spectra representing the distribution of elements in the depth direction for NiO, NiO/**PRuV**, and NiO/**PRu-*poly*-Ru-N^N**. The observed Ru^+ species throughout the entire range for NiO/**PRuV** and NiO/**PRu-*poly*-Ru-N^N** indicate that the Ru complex penetrates the NiO film layer. The amount of Ru in the NiO is within the error range of the detector.

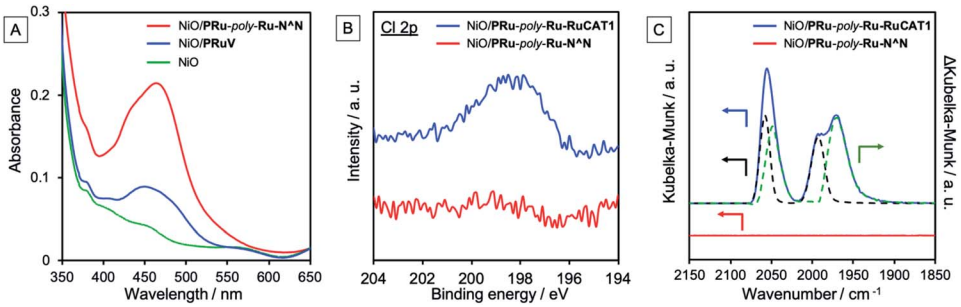

Fig. 5 (A) UV-vis absorption spectra of the NiO/**PRu**-*poly*-**Ru-N^N** (red line), NiO/**PRuV** (blue line), and NiO electrodes (green line). FTO electrode was employed as the background. (B) X-ray photoelectron spectroscopy (XPS) spectra of NiO/**PRu**-*poly*-**Ru-RuCAT1** (blue line) and NiO/**PRu**-*poly*-**Ru-N^N** (red line). (C) FT-IR spectra of NiO/**PRu**-*poly*-**Ru-RuCAT1** (blue line) and NiO/**PRu**-*poly*-**Ru-N^N** (red line). The spectrum of **Ru-RuCAT** on the NiO electrode (black dotted line), and the differential spectrum between NiO/**PRu**-*poly*-**Ru-RuCAT1** and **Ru-RuCAT** (green dotted line). A diffuse reflection unit was utilized for the measurements, with a bare NiO electrode employed as the background.

which is attributed to the singlet metal-to-ligand-charge-transfer (^{1}MLCT) absorption band of the Ru photosensitizer unit (Fig. 5A, S1†). This absorbance of NiO/**PRu**-*poly*-**Ru-N^N** is significantly higher than that of NiO/**PRuV**. These results demonstrate that the electropolymerized complexes maintained the structure of the Ru photosensitizer unit in NiO/**PRu**-*poly*-**Ru-N^N**, and more photosensitizer units were introduced into and on the electrode by the electropolymerization compared to those involving only methyl phosphonic acid groups, *i.e.*, NiO/**PRuV**.

The $Ru^{II}(N^N)(CO)_2Cl_2$-type catalyst was formed with the non-coordinated diimine ligand of the NiO/**PRu**-*poly*-**Ru-N^N** electrode by dipping the electrode into an MeCN solution containing $[Ru(CO)_2Cl_2]_n$ as a precursor for 1–2 day(s). No difference is obvious between the UV-vis absorption spectra of the electrode before (NiO/**PRu**-*poly*-**Ru-N^N**, Fig. S2†) and after introducing the catalyst (NiO/**PRu**-*poly*-**Ru-RuCAT1**). This is reasonable because the $Ru^{II}(N^N)(CO)_2Cl_2$-type complexes exhibit only weak or no absorption in this range (Fig. S1†). Fig. 5B and C show spectra from X-ray photoelectron spectroscopy (XPS) and FT-IR, respectively. The XPS spectrum of NiO/**PRu**-*poly*-**Ru-RuCAT1** displays a peak attributed to Cl 2p, which is not observed for NiO/**PRu**-*poly*-**Ru-N^N**, indicating introduction of the Ru catalyst units into the electrode. The FT-IR spectrum for NiO/**PRu**-*poly*-**Ru-RuCAT1** shows three prominent broad peaks at 2056 cm^{-1}, 1993 cm^{-1}, and 1976 cm^{-1} attributed to carbonyl stretching vibrations, whereas none is observed for NiO/**PRu**-*poly*-**Ru-N^N**. The peak at 1993 cm^{-1} corresponds to the *cis*-(CO)-*trans*-(Cl)–$Ru(N^N)(CO)_2Cl_2$ vibration, consistent with that of [*cis*-(CO)-*trans*-(Cl)–$Ru(dmb)_2$(bpyC$_2$bpy)$Ru(CO)_2Cl_2](PF_6)_2$ (**Ru-RuCAT**: dmb = 4,4′-dimethyl-2,2′-bipyridyl) drop-cast on the NiO electrode (black dotted line in Fig. 5C). The difference spectrum between NiO/**PRu**-*poly*-**Ru-RuCAT1** and **Ru-RuCAT** (2058, 1991 cm^{-1}) gives two peaks at 2049 and 1970 cm^{-1}, suggesting the formation of another Ru(II) complex with the carbonyl ligands. This is likely a *cis*-(CO)-*cis*-(Cl)–$Ru(N^N)(CO)_2Cl_2$-type complex, because such an isomer is known as a by-product in the synthesis of *cis*-(CO)-*trans*-(Cl)–$Ru(N^N)(CO)_2Cl_2$, and displays two CO vibrational peaks with lower wavenumbers than those of *cis*-(CO)-*trans*-(Cl)–$Ru(dmb)(CO)_2Cl_2$.[26–28] From these results, we concluded that Ru catalyst units were introduced through coordination bonds with the free diimine unit of NiO/**PRu**-*poly*-**Ru-N^N**. Note that *cis*-

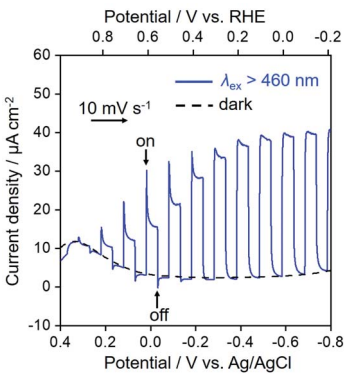

Fig. 6 Current–potential curves of NiO/**PRu**-*poly*-**Ru-RuCAT1** (electrode area: 2.5 cm^2) as the working electrode in a CO_2-purged $NaHCO_3$ (50 mM) aqueous solution (pH = 6.6). The scan rate is 10 mV s^{-1} with intermittent light at 460 nm < λ_{ex} < 650 nm (27 mW cm^{-2}), and irradiated from the back side of the electrode.

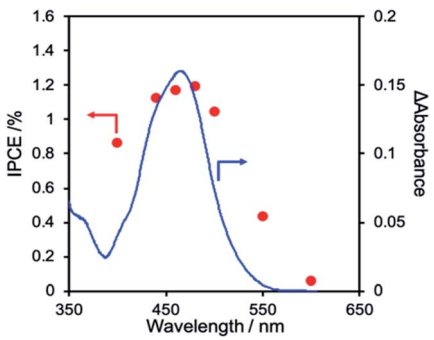

Fig. 7 Action spectrum of the IPCE of NiO/**PRu**-*poly*-**Ru-RuCAT1** at −0.7 V *vs.* Ag/AgCl (−0.11 V *vs.* RHE) in a CO_2-purged 50 mM $NaHCO_3$ aqueous solution (pH = 6.6) (red dots). The blue line represents the UV-vis absorption spectrum of NiO/**PRu**-*poly*-**Ru-RuCAT1** after subtracting the absorbance of the NiO electrode.

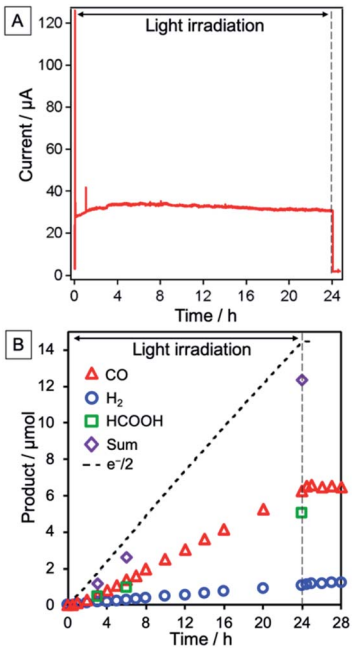

Fig. 8 (A) Time courses of photocurrent and (B) products, *i.e.*, CO (red triangles), HCOOH (green squares), and H_2 (blue circles). Half of the flowing electrons are also shown (black dotted line). NiO/**PRu**-*poly*-**Ru**-**RuCAT1** (electrode area: 2.5 cm^2) with applied bias at $E = -0.7$ V *vs.* Ag/AgCl (−0.11 V *vs.* RHE) was irradiated at 460 nm < λ_{ex} < 650 nm (27 mW cm^{-2}) in a CO_2-purged 50 mM $NaHCO_3$ aqueous solution (pH = 6.6).

(CO)-*cis*-(Cl)–Ru(N^N)$(CO)_2Cl_2$ also acts as a CO_2 reduction catalyst like isomer *cis*-(CO)-*trans*-(Cl)–Ru(N^N)$(CO)_2Cl_2$.[26,27]

The total amounts of the Ru photosensitizer and the Ru catalyst on the electrode are 34 and 15 nmol cm^{-2}, respectively (see Experimental for calculation details).

Photoelectrochemical properties

Fig. 6 shows the current–potential curves of NiO/**PRu**-*poly*-**Ru**-**RuCAT1** in a CO_2-purged aqueous solution containing $NaHCO_3$ (50 mM) during irradiation at λ_{ex} > 460 nm or under dark conditions. Under the irradiation, the cathodic photocurrent was observed from $E = \sim$+0.3 V *vs.* Ag/AgCl, and increased with scanning to a more negative potential. A reasonable agreement exists between the action spectrum of the incident photon to current conversion efficiency (IPCE) and the UV-vis absorption spectrum of the Ru photosensitizer unit on NiO/**PRu**-*poly*-**Ru**-**RuCAT1** (Fig. 7). This suggests that the cathodic photocurrent is generated by the photoexcitation of the Ru photosensitizer unit. The maximum IPCE of NiO/**PRu**-*poly*-**Ru**-**RuCAT1** is 1.2% at $E = -0.7$ V *vs.* Ag/AgCl under irradiation at $\lambda_{ex} = 480$ nm.

Photoelectrochemical CO_2 reduction

The NiO/**PRu**-*poly*-**Ru**-**RuCAT1** electrode at an applied bias of −0.7 V *vs.* Ag/AgCl (corresponding to −0.11 V *vs.* RHE), irradiated at λ_{ex} > 460 nm under a CO_2 atmosphere, yielded CO and HCOOH as main products, and H_2 as a by-product. Fig. 8A shows the time course of the photocurrent for 24 h of irradiation, without any decrease even after 24 h. The formation rate of reduction products was also maintained during the 24 h (Fig. 8B), with turnover numbers (TONs) 176, 135, and 30 for CO (6.5 μmol), HCOOH (5.0 μmol), and H_2 (1.1 μmol), respectively after 24 h irradiation (see Experimental for calculation details). The carbon source of the produced CO and HCOOH was confirmed as CO_2 by $^{13}CO_2$ isotope-labelling experiments (Fig. 9). The faradaic efficiency (F_{red}, 87%) and the selectivity of CO_2 reduction (91%) were very high even in the aqueous solution.

Almost no change was observed in the UV-vis absorption spectrum of the photocathode even after 24 h irradiation (Fig. 10A). This indicates no decomposition or desorption of the Ru photosensitizer unit from the electrode during the photocatalytic reaction, highlighting durable photoelectrochemical CO_2 reduction. XPS and FT-IR spectroscopy were used for checking the **RuCAT1** units of the photoelectrode after the photocatalytic reaction. The XPS spectrum was characterized by disappearance of the Cl 2p peak (Fig. 10B). Although CO stretching bands with similar strengths are present in the FT-IR spectrum, their wavenumbers changed to 2030, and 1955 cm^{-1} (Fig. 10C). These results indicate substitution of the Cl ligands

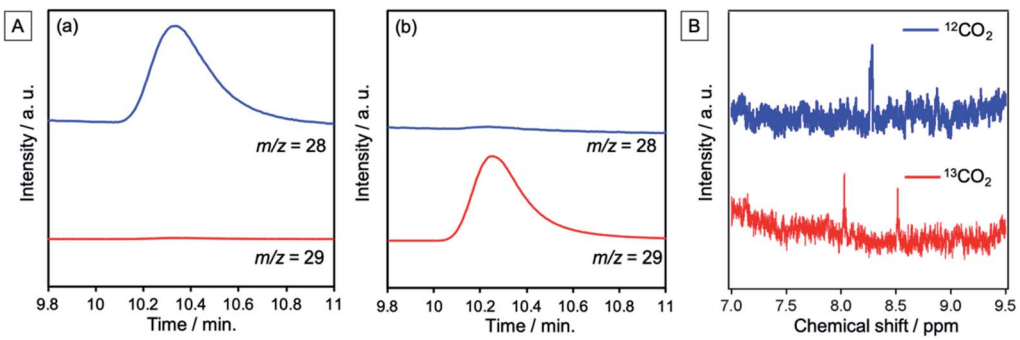

Fig. 9 (A) GC-MS chromatograms of the gas phase in the reaction cell after irradiation, showing peaks at $m/z = 28$ for ^{12}CO and 29 for ^{13}CO. NiO/**PRu**-*poly*-**Ru**-**RuCAT1** with applied bias at $E = -0.7$ V *vs.* Ag/AgCl (−0.11 V *vs.* RHE) was irradiated at λ_{ex} > 460 nm in a CO_2-purged 50 mM $NaHCO_3$ aqueous solution (pH = 6.6) for 24 h using (a) regular CO_2 and $NaHCO_3$ and (b) $^{13}CO_2$ and $NaH^{13}CO_3$. (B) ^1H NMR spectra of the solution after the photoelectrochemical reaction. NiO/**PRu**-*poly*-**Ru**-**RuCAT1** at $E = -0.7$ V *vs.* Ag/AgCl (−0.11 V *vs.* RHE) was irradiated at λ_{ex} > 460 nm in a CO_2-purged 50 mM $NaHCO_3$ aqueous solution (pH = 6.6) for 24 h using regular CO_2 and $NaHCO_3$ (blue line) or $^{13}CO_2$ and $NaH^{13}CO_3$ (red line).

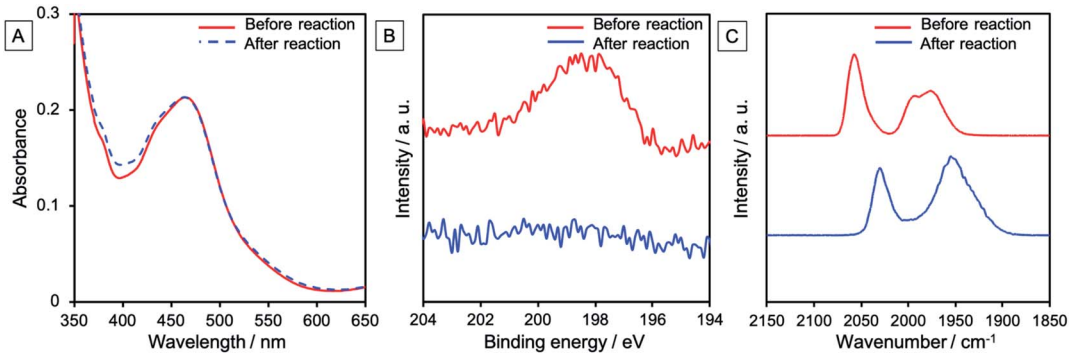

Fig. 10 (A) UV-vis absorption spectra of NiO/**PRu**-*poly*-**Ru**-**RuCAT1** before (red line) and after (blue dotted line) photoelectrochemical CO_2 reduction for 24 h, with an FTO electrode employed as the background. (B) The XPS Cl 2p spectra of NiO/**PRu**-*poly*-**Ru**-**RuCAT1** before (red line) and after (blue line) the reaction. (C) FT-IR spectra of NiO/**PRu**-*poly*-**Ru**-**RuCAT1** before (red line) and after (blue line) the reaction. A diffuse reflection unit was used for the measurements and the background was measured using a bare NiO electrode.

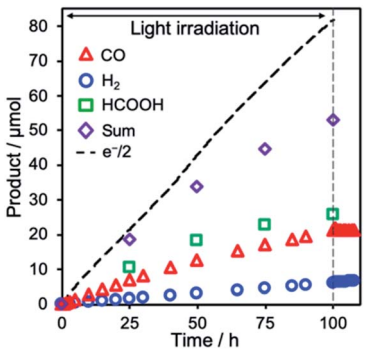

Fig. 11 Time courses of the produced CO (red triangle), H_2 (blue circle), and HCOOH (green square), and half of the flowing electrons (black dotted line) during irradiation of NiO/**PRu**-*poly*-**Ru**-**RuCAT1** (electrode area: 2.5 cm^2) at $E = -0.7$ V *vs.* Ag/AgCl (−0.11 V *vs.* RHE) in a CO_2-purged 50 mM $NaHCO_3$ aqueous solution (pH = 6.6) under 460 nm < λ_{ex} < 650 nm, 27 mW cm^{-2}.

of the **RuCAT1** unit with other ligands, which is consistent with previous reports describing the behaviours of $Ru(N\hat{}N)(CO)_2Cl_2$-type catalysts during photocatalytic CO_2 reduction reactions in homogeneous solutions.[29] The shifts toward lower wavenumbers of the peaks in the FT-IR spectrum reflect coordination of higher electron donating ligands than Cl^-, such as $HCOO^-$ and/or OH^-. It is noteworthy that the Ru(0) polymer $[Ru(diimine)(CO)_2]_n$ which shows ν_{CO} bands at 2035 and 2084 cm^{-1} was not observed. Although such polymerization of the $[Ru(diimine)(CO)_2Cl_2]$ type complexes during photocatalytic reduction of CO_2 in homogeneous solutions was reported as a deactivation process of the photocatalysis, in the photoelectrochemical system, the Ru complexes cannot freely move on the electrode resulting in suppression of this deactivation process of the Ru catalyst unit.

Remarkably, photocatalytic CO_2 reduction continued even after 100 h irradiation (Fig. 11). Although the faradaic efficiency gradually decreased to 65% after 100 h irradiation because of the slow penetration of air into the closed cell and resulting electron consumption *via* the reduction of O_2, production of CO and HCOOH continued without significant reduction in their selectivity (entries 1–3 in Table 1). The total TON of the photocatalytic CO_2 reduction exceeded 1200 (TON_{CO} = 576, TON_{HCOOH} = 695, TON_{H_2} = 172), representing the highest TON

Table 1 Photoelectrochemical reactions using various electrodes under varying conditions[a]

		Irradn. time	E		Products/μmol (F_{red})				
Entry	Electrode	h	$V_{Ag/AgCl}$[b]	V_{RHE}[c]	CO	HCOOH	H_2	Total	$e^-/2$
1	NiO/**PRu**-*poly*-**Ru**-**RuCAT1**	5	−0.7	−0.11	1.1 (35)	1.2 (39)	0.2 (6)	2.5 (81)	3.1
2	NiO/**PRu**-*poly*-**Ru**-**RuCAT1**	24	−0.7	−0.11	6.5 (45)	5.0 (34)	1.1 (8)	12.6 (87)	14.5
3	NiO/**PRu**-*poly*-**Ru**-**RuCAT1**	100	−0.7	−0.11	21.3 (26)	25.7 (31)	6.3 (8)	53.3 (65)	82.0
4	NiO/**PRu**-*poly*-**Ru**-**RuCAT1**	5	−0.3	+0.29	0.7 (32)	0.9 (41)	0.1 (5)	1.7 (77)	2.2
5	NiO/**PRu**-*poly*-**Ru**-**RuCAT1**	5	0	+0.59	0.1 (18)	0.3 (37)	0.05 (7)	0.5 (62)	0.8
6	NiO/**PRu**-*poly*-**Ru**-**N^N**	5	−0.7	−0.11	Trace	0.1 (13)	0.3 (38)	0.4 (49)	0.8
7	NiO/**PRu**-**RuCAT**	5	−0.7	−0.11	0.03 (5)	0.2 (45)	0.05 (9)	0.3 (59)	0.5
8	NiO/**PRu**-*poly*-**Ru**-**RuCAT2**	5	−0.7	−0.11	1.2 (43)	0.5 (18)	0.2 (7)	1.9 (67)	2.8
9	NiO/**PRu**-*poly*-**Ru**-**RuCAT2**	24	−0.7	−0.11	5.5 (58)	1.1 (12)	0.3 (3)	6.9 (73)	9.5
10[d]	NiO/**PRu**-*poly*-**Ru**-**Re**	5	−0.7	−0.11	0.5 (55)	0.1 (13)	0.2 (17)	0.8 (85)	0.9
11	NiO	5	−0.7	−0.11	n. d.[e]	n. d.[e]	0.01 (5)	0.01 (5)	0.2

[a] Electrodes (electrode area: 2.5 cm^2) in aqueous solutions containing $NaHCO_3$ (50 mM, pH = 6.6) irradiated at 460 nm < λ_{ex} < 650 nm using a 300 W Xe lamp (27 mW cm^{-2}). [b] *vs.* Ag/AgCl (sat. KCl aq). [c] *vs.* RHE. [d] Data from ref. 7. [e] n.d.: not detected.

reported for CO_2 reduction using molecular photocathodes, to the best of our knowledge.

Although the cathodic current and the generated products decreased when the applied bias shifted to more positive *i.e.*, at $E = -0.3$ V and 0 V (entries 4 and 5 in Table 1, Fig. S3†), the NiO/**PRu-*poly*-Ru-RuCAT1** photocathode still drove the reaction to produce CO and HCOOH. Notably, the potential of 0 V *vs.* Ag/AgCl (corresponding to +0.59 V *vs.* RHE), at which the photocathode could generate the detectable products, was more positive than previously reported molecular photocathodes based on NiO, containing the Re(N^N)$(CO)_3$Br-type complex as the catalyst unit. The photoelectrochemical properties are compared between these photocathodes in Fig. S4.†[5,7,20] This difference in the practicable potential possibly originates from different catalytic properties of Ru(N^N)$(CO)_2Cl_2$ including more positive reduction potential compared to the Re(N^N)$(CO)_3$Br catalyst. This positive shift of the onset potential is advantageous for the CO_2 reduction combined with the photoanode for water oxidation.

Effects of assembly methods of the photocathodes on the activity for CO_2 reduction

NiO/**PRu-*poly*-Ru-N^N** without the catalyst unit hardly proceeded photocatalytic CO_2 reduction under 5 h irradiation (entry 6 in Table 1). The decomposition of the Ru photosensitizer unit would produce $[Ru(N^N)_2(L)(L')]^{2+}$-type complexes, which generate HCOOH at very low efficiency in cooperation with the residual Ru photosensitizer units.[25,30] This clearly indicates that the Ru catalyst unit is crucial in the photocatalytic CO_2 reduction (Table 1, entry 1 for comparison). It is noteworthy that CO or HCOOH was not detected using a bare NiO electrode (entry 11).

Two methods were applied for synthesizing molecular photocathodes comprising similar metal complex units, *i.e.*, $[Ru(N^N)_3]^{2+}$-type photosensitizer and Ru(N^N)$(CO)_2Cl_2$-type catalyst units on the NiO electrode. These include: (1) adsorption of the Ru(II)–Ru(II) supramolecular photocatalyst with methyl phosphonic acid groups (**PRu-RuCAT**, Fig. 12) directly onto the NiO surface (NiO/**PRu-RuCAT**, Scheme 2a) and (2) electropolymerization of the Ru(II)–Ru(II) supramolecular photocatalyst with vinyl groups on the photosensitizer unit (**VRu-RuCAT**, Fig. 12) on NiO/**PRuV** (NiO/**PRu-*poly*-Ru-RuCAT2**, Scheme 2b). These methods were reported for the synthesis of molecular photocathodes with another supramolecular photocatalyst containing the $[Ru(N^N)_3]^{2+}$-type photosensitizer and

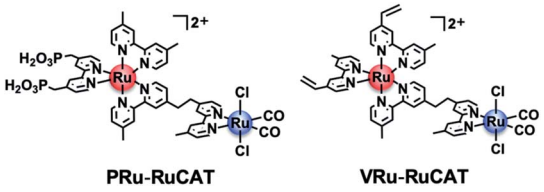

Fig. 12 Chemical structures of the metal complexes used for the synthesis of NiO/PRu-RuCAT and NiO/PRu-*poly*-Ru-RuCAT2.

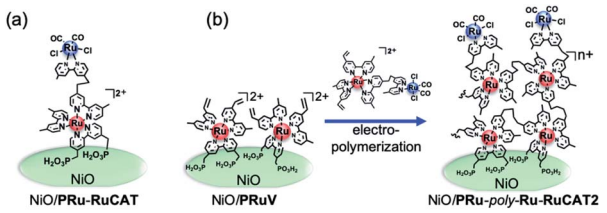

Scheme 2 Preparation scheme for (a) NiO/PRu-RuCAT and (b) NiO/PRu-*poly*-Ru-RuCAT2.

Re(N^N)$(CO)_3$Br-type catalyst units (NiO/**PRu-Re**[4,5] and NiO/**PRu-*poly*-Ru-Re**,[7] respectively, shown in Scheme S1†).

Fig. 13 shows the time courses of photocurrent during photoelectrochemical CO_2 reduction using these electrodes and NiO/**PRu-*poly*-Ru-RuCAT1** as well. Although lower photocurrent was observed for NiO/**PRu-RuCAT**, it rapidly declined within a few hours. This small photocurrent and low stability reflect a similar tendency for the previously reported NiO/**PRu-Re**.[4,5] These characteristics are attributed to the low adsorption density of the supramolecular photocatalysts and low adsorption stability of the methyl phosphonic acid anchors on the NiO surface. Much smaller amounts of CO_2-reduction products were produced using NiO/**PRu-RuCAT** compared to products using NiO/**PRu-*poly*-Ru-RuCAT1** (entries 7 and 1 in Table 1 for comparison).

In the initial stage of the photocatalytic reaction using NiO/**PRu-*poly*-Ru-RuCAT2**, the photocurrent was similar to that using NiO/**PRu-*poly*-Ru-RuCAT1**, however, the current value gradually decreases from 45 to 15 μA during 24 h irradiation (Fig. 13). The total amounts of CO and HCOOH produced were lower compared to those using NiO/**PRu-*poly*-Ru-RuCAT1** after 24 h irradiation (entries 2 and 9 in Table 1 for comparison). The UV-vis absorption spectrum of NiO/**PRu-*poly*-Ru-RuCAT2** after the reaction showed a decrease in the absorption of the Ru photosensitizer unit (Fig. 14A). In addition, the UV-vis spectrum of the reaction solution after 5 h irradiation clearly indicates the

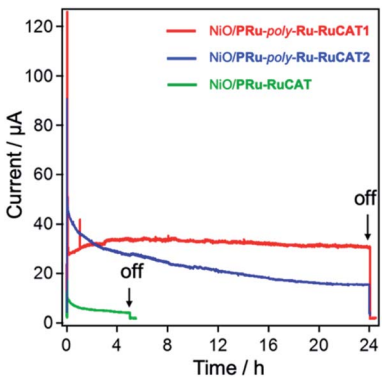

Fig. 13 Time courses of the photocurrent using NiO/PRu-*poly*-Ru-RuCAT1 (red line), NiO/PRu-*poly*-Ru-RuCAT2 (blue line), and NiO/PRu-RuCAT (green line) at $E = -0.7$ *vs.* Ag/AgCl (−0.11 V *vs.* RHE), irradiated at 460 nm < λ_{ex} < 650 nm (27 mW cm^{-2}) in a CO_2-purged 50 mM $NaHCO_3$ aqueous solution (pH = 6.6). The active areas of all electrodes were 2.5 cm^2.

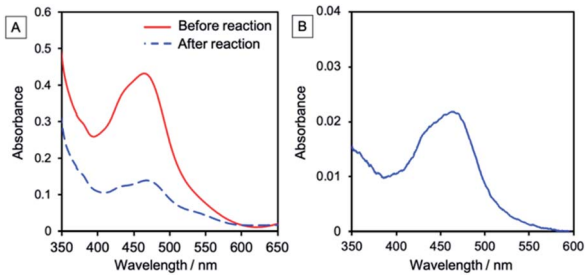

Fig. 14 (A) UV-vis absorption spectra of NiO/**PRu**-*poly*-**Ru-RuCAT2** before (red line) and after (blue dotted line) the photoelectrochemical CO_2 reduction for 24 h, with an FTO electrode employed as the background. (B) UV-vis absorption spectrum of the reaction solution after photoelectrochemical CO_2 reduction using NiO/**PRu**-*poly*-**Ru-RuCAT2** for 5 h.

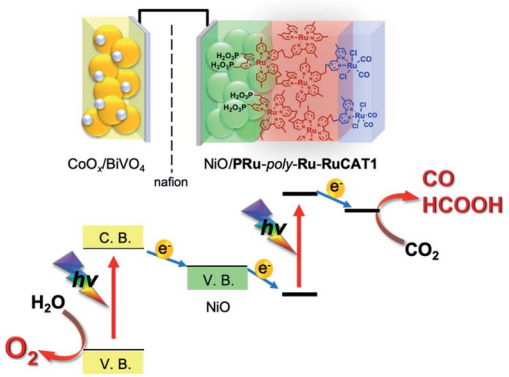

Scheme 3 Photoelectrochemical CO_2 reduction with water as a reductant and visible light as the energy source by a cell comprising the NiO/**PRu**-*poly*-**Ru-RuCAT1** photocathode and $CoO_x/BiVO_4$ photoanode.

desorption of the Ru(II) complexes from the molecular photocathode to the solution (Fig. 14B). These results suggest that the desorption of some parts of the metal complexes from the electrode leads to the decrease of the photocurrent, as shown in Fig. 13. The FT-IR spectrum of NiO/**PRu**-*poly*-**Ru-RuCAT2** differed from that of **VRu-RuCAT** (Fig. S5†), suggesting that the structure of the $Ru(N^N)(CO)_2Cl_2$ catalyst unit changed during the electropolymerization. The SEM observations reveal that the polymer film of NiO/**PRu**-*poly*-**Ru-RuCAT2** mainly attached on the surface of the NiO film (Fig. S6B†), which was different for NiO/**PRu**-*poly*-**RuCAT1** (Fig. S6A†) but similar for the reported NiO/**PRu**-*poly*-**Ru-Re** (Fig. S6C†).[7] The bulkiness of **VRu-RuCAT** compared to **VRu-N^N** probably suppressed polymerization within the NiO film. The previous study for NiO/**PRu**-*poly*-**Ru-Re** suggests that the Re catalyst unit released its Br ligand and coordinated with radical species produced from the vinyl group during the electropolymerization, which partially contributed to producing the polymer structure. A similar reaction, *i.e.*, Ru–C bond formation, is expected in the synthesis of NiO/**PRu**-*poly*-**Ru-RuCAT2**. The cleavage of this Ru–C bond and the surface localization of the **Ru-RuCAT2** unit on the surface of NiO/**PRu**-*poly*-**Ru-RuCAT2** probably contributed to eliminating the Ru(II) complexes from the electrode surface during the photocatalytic reduction of CO_2. These results clearly highlight the advantage of the newly reported preparation method for NiO/**PRu**-*poly*-**Ru-RuCAT1**, *i.e.*, the stepwise method (electropolymerization and the subsequent introduction of the catalyst unit) successfully prevents the decline of photocatalysis of the molecular photocathode mainly owing to the suppression of the detachment of the molecular photocatalysts from the electrode.

Photoelectrochemical CO_2 reduction with water oxidation

Since NiO/**PRu**-*poly*-**Ru-RuCAT1** showed the highest photocatalysis for CO_2 reduction for the reported molecular photocathodes, a photoelectrochemical cell comprising NiO/**PRu**-*poly*-**Ru-RuCAT1** with a photoanode for water oxidation was constructed for reducing CO_2 with water as an electron donor (Scheme 3). We selected a CoO_x-deposited $BiVO_4$ electrode ($CoO_x/BiVO_4$), which has good activity for water oxidation under visible light irradiation, enough stability, and a sufficiently negative conduction band to pass electrons to the valence band of NiO.[31,32] The photoelectrochemical properties of the $CoO_x/BiVO_4$ photoanode were examined using the same solution for the CO_2 reduction reaction, *i.e.*, the CO_2-purged water solution containing 50 mM $NaHCO_3$ (pH = 6.6). Fig. 15A shows the current–potential curve during irradiation at 400 nm < λ_{ex} < 650 nm (40 mW cm^{-2}); photoanodic current was generated and the onset potential was much more negative than +0.3 V (*vs.* Ag/AgCl) which is the onset potential of the NiO/**PRu**-*poly*-**Ru-RuCAT1** photocathode. Fig. 15B shows the time course of photocurrent under continuous light irradiation (the same reaction conditions described above); stable photoanodic current was observed for 1 h irradiation at $E = 0$ V *vs.* Ag/AgCl, and the evolution of O_2 was confirmed during the irradiation with a reasonable faradaic efficiency ($F = 75\%$).

A photoelectrochemical cell consisting of the NiO/**PRu**-*poly*-**Ru-RuCAT1** molecular photocathode and $CoO_x/BiVO_4$ photoanode separated by a Nafion membrane was constructed as

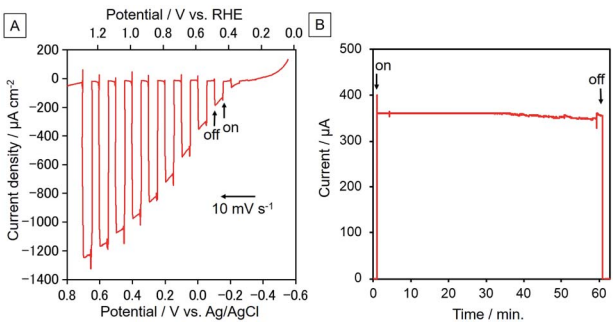

Fig. 15 (A) Current–potential curve of $CoO_x/BiVO_4$ (electrode area: 1.3 cm^2) as a working electrode in a CO_2-purged $NaHCO_3$ (50 mM) aqueous solution (pH = 6.6) with intermittent irradiation. The scan rate is 10 mV s^{-1} with light at 400 nm < λ_{ex} < 650 nm (40 mW cm^{-2}), with the electrode irradiated from the front side. (B) Time courses of the photocurrent from the $CoO_x/BiVO_4$ electrode at $E = 0$ V *vs.* Ag/AgCl (+0.59 V *vs.* RHE). The same light and solution were used as described in (A).

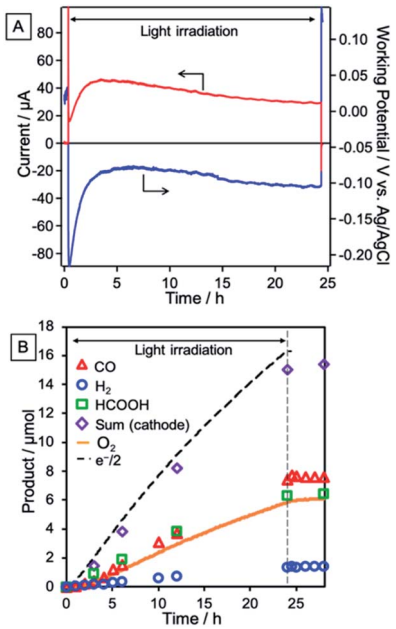

Fig. 16 Time courses of (A) photocurrent (red line) and the working potential of the electrode (blue line) and (B) products during visible light irradiation (cathode: 480 nm < λ_{ex} < 650 nm, 81 mW cm^{-2}, anode: 400 nm < λ_{ex} < 650 nm, 61 mW cm^{-2}) by the photoelectrochemical cell comprising the NiO/**PRu**-*poly*-**Ru**-**RuCAT1** photocathode and CoO_x/$BiVO_4$ photoanode without bias in a CO_2-purged $NaHCO_3$ (50 mM) aqueous solution (pH = 6.6).

illustrated in Scheme 3. The NiO/**PRu**-*poly*-**Ru**-**RuCAT1** and CoO_x/$BiVO_4$ electrodes were irradiated with visible light (480 nm < λ_{ex} < 650 nm, 81 mW cm^{-2} and 400 nm < λ_{ex} < 650 nm, 61 mW cm^{-2}, respectively) without any applied bias in a CO_2-purged $NaHCO_3$ (50 mM) aqueous solution (pH = 6.6), and the photocurrent was observed for 24 h (Fig. 16A). The photocurrent increased initially, reaching its maximum after 3.5 h, similar to the half reaction using NiO/**PRu**-*ply*-**Ru**-**RuCAT1** (Fig. 8A and S3†). This would be caused by the structural change of the **RuCAT1** catalyst unit in the photocathode. It is noteworthy that about 65% of the photocurrent was maintained even after the 24 h irradiation compared to the maximum. For 24 h, CO (8.0 μmol, TON_{CO} = 219) and HCOOH (6.4 μmol, TON_{HCOOH} = 175) continuously formed as main products in the cathode chamber, with a lower amount of H_2 (1.4 μmol) generated (Fig. 16B). In addition, O_2 (6.1 μmol) was also continuously produced as a main product in the anode chamber (Fig. 16B). The faradaic efficiencies of the cathode and anode are 97% and 75%, respectively. These results demonstrate that stable CO_2 reduction using water as the reductant and visible light as the energy source for 24 h proceeded as the main reaction. The slightly lower faradaic efficiency for O_2 evolution in the anode chamber is probably caused by the formation of H_2O_2 as another product of the water oxidation, as previously reported for a similar photoelectrochemical system using $BiVO_4$ with a bicarbonate electrolyte.[33,34] The energy conversion efficiency was 1.7 × 10^{-2}% for 24 h irradiation, which is the highest value reported for full cells using molecular photocatalysts for not only CO_2 reduction but also H_2 evolution.[35–37] Table 2 summarizes photocatalyses of the reported non-biased full photoelectrochemical cells, which used a molecular photocatalyst for CO_2 reduction or H_2 evolution, coupled with water oxidation, and our system reported in this paper is also included.

Experimental

General procedures

The ^{1}H NMR spectra were measured in acetonitrile-d_3 using a JEOL ECA400-II system at 400 MHz. Transmission IR spectra in CH_2Cl_2 were measured using a JASCO FT/IR-6600 spectrometer at 1 cm^{-1} while diffuse reflectance IR spectra were obtained using a diffuse reflectance unit (DR-81, JASCO) at 2 cm^{-1}. Since it was hard to obtain the transmission IR spectra of the electrodes due to the absorption and roughness of the support NiO, we employed diffuse reflection IR spectroscopy. Electrospray ionization-mass spectroscopy (ESI-MS) was performed using a Shimadzu LC-MS-2010 A system with acetonitrile (MeCN) as the mobile phase. Electrospray ionization time-of-flight mass spectroscopy (ESI-TOF-MS) was performed using a Waters LCT Premier mass spectrometer with MeOH as the mobile phase. Scanning electron microscopy (SEM) images were obtained using a Hitachi S4700. Gas chromatography-mass spectrometry (GC-MS) was performed with a Shimadzu QP-2010-Ultra. TOF-SIMS was conducted with an ION-TOF GmbH TOF-SIMS 5-100-AD. The UV-vis absorption spectra were recorded with a JASCO V-565 instrument. The X-ray photoelectron spectroscopy (XPS) measurements were conducted using an ESCA-3400 (Shimadzu). The binding energy of the impurity of the carbon (1 s) peak was adjusted to 285.0 eV to correct the chemical shift of each element.

Materials

MeCN was distilled twice after refluxing over P_2O_5 overnight, and then distilled over CaH_2 immediately before use. Et_4NBF_4 was recrystallized from MeCN/ethyl acetate, and then dried under reduced pressure at 373 K overnight before utilization. The $^{13}CO_2$ (^{13}C = 99%) was purchased from Cambridge isotope laboratories Inc., while $NaH^{13}CO_3$ (^{13}C = 98%) was purchased from Aldrich. $[Ru(vbpy)_2\{(H_2O_3PCH_2)_2bpy\}](PF_6)_2$ (**PRuV**) (vbpy = 4-methyl-4′-vinyl-2,2′-bipyridine),[7] $[Ru(vbpy)_2(bpyC_2bpy)](PF_6)_2$ (**VRu-N^N**),[7] $[Ru(CO)_2Cl_2]_n$,[38] and $[Ru(dmb)\{(H_2O_3PCH_2)_2bpy\}(bpyC_2bpy)Ru(CO)_2Cl_2](PF_6)_2$ (**PRu-RuCAT**)[38] were prepared according to literature procedures with some modifications. Other reagents and solvents were of commercial grade quality and were used without further purification.

Synthesis of VRu-RuCAT2 ($[Ru(vbpy)_2(bpyC_2bpy)Ru(CO)_2Cl_2](PF_6)_2$)

VRu-N^N (17.6 mg, 0.0153 mmol) and $[Ru(CO)_2Cl_2]_n$ (3.47 mg, 0.0152 mmol) were dissolved in CH_2Cl_2 (10 mL) and refluxed for 2 h. After evaporation of the solvent, the residue was recrystallized from CH_2Cl_2/Et_2O. The obtained red-orange solid was dried under vacuum. Yield: 11.6 mg (55%). FT-IR (in CH_2Cl_2)

Table 2 Comparison of the non-biased full photoelectrochemical cells using a molecular photocatalyst coupled with water oxidation

Photocathode, Photoanode	Irradiance for each electrode/ mW cm^{-2}	Average current	Reaction time/h	Products from each electrode (F_{red}/%)	Energy conversion efficiency/%	Ref.
NiO/**PRu-*poly*-Ru-RuCAT1**, CoO_x/$BiVO_4$	81, 61	37[a]	24	CO (49) + HCOOH (39) + H_2 (9), O_2 (75)	1.7×10^{-2}	This work
RuRe/$CuGaO_2$, CoO_x/TaON	Not described	~20[a]	2	CO (31) + H_2 (42), O_2 (70)	—	6
NiO|**PMI-6T-TPA**, $BiVO_4$	Not described	2.7[b]	2	H_2 (80)	—	35
NiO|**P1**|**Co**, TiO_2|**L0**|**Ru1**	100, 100	15[b]	1.7	H_2 (55)	5.1×10^{-3}	36[c]
$CuGaO_2$|**RBG174**|**CoHEC**, TaON/CoO_x	30, 50	10.3[a]	2	H_2 (87), O_2 (88)	5.4×10^{-3}	37

[a] Absolute current from the cell (μA). [b] Current density (μA cm^{-2}). [c] The data were recalculated in ref. 37.

ν_{CO}/cm^{-1}: 2062, 2000. ESI-MS (in MeCN): m/z = 544 [M − $2PF_6^-$]$^{2+}$. ^{1}H NMR (400 MHz, acetonitrile-d_3): δ/ppm 8.92–8.87 (m, 2H), 8.39–8.17 (m, 8H), 7.57–7.08 (m, 14H), 6.81–6.74 (m, 2H, –C*H* = CH_2), 6.24–6.19 (m, 2H, –CH = CH_2(*cis*)), 5.65–5.62 (m, 2H, –CH = CH_2(*trans*)), 3.23–3.20 (m, 4H), 2.50–2.40 (m, 12H). HRMS (ESI-TOF, in MeOH) m/z: [M − $2PF_6^-$]$^{2+}$ calcd for $C_{52}H_{46}Cl_2N_8O_2Ru_2$: 544.0612; found: 544.0609.

Fabrication of the NiO electrode

The NiO electrode was prepared according to procedures in the literature.[4] The outline of the preparation is as follows: The precursor solution of water–EtOH (4.5 g, 1 : 2, w/w) and a solution containing $Ni(NO_3)_2 \cdot 6H_2O$ (1.0 g, 99.95%, Kanto chemicals) and Pluronic F-88 (0.5 g) were deposited onto a clean FTO glass (AGC fabritech, 15 × 50 mm^2, 12 Ω sq^{-1}) by the squeegee method. The sample was calcined at 773 K for 0.5 h in air, and this deposition–calcination cycle was repeated four times. This electrode was then cut in half before use (electrode area: 2.5 cm^2).

Preparation of NiO/PRuV or NiO/PRu-RuCAT by adsorption through a phosphonic acid anchor

The NiO electrode (electrode area: 2.5 cm^2) was soaked in an MeCN solution (4 mL) containing **PRuV** or **PRu-RuCAT** (5 μM) overnight. The electrode was washed with MeCN and dried under dark conditions. The amount of the adsorbed metal complex on the NiO electrode was calculated from the difference of the absorbance of the solution at the absorption maximum of the ^{1}MLCT absorption band, before and after the adsorption.

Electropolymerization of VRu-N^N or VRu-RuCAT2 onto NiO/PRuV

An MeCN solution (5 mL) containing **VRu-N^N** or **VRu-RuCAT2** (0.5 mM) and Et_4NBF_4 (0.1 M) was added to a one-component electrochemical cell, with NiO/**PRuV** as the working electrode. An $Ag/AgNO_3$ reference electrode (Ag wire immersed in MeCN containing 10 mM $AgNO_3$ and 0.1 M Et_4NBF_4 separated by vycol® from the electrolyte solution) and a platinum-wire were used as the reference and the counter electrodes, respectively. After purging with Ar for 10 min, the potential was swept between 0 to −1.9 V *vs.* $Ag/AgNO_3$ at 100 mV s^{-1}. The obtained electrodes were washed with pure MeCN and stored in the dark.

Introduction of the Ru catalyst unit into NiO/PRu-*poly*-Ru-N^N

NiO/**PRu-*poly*-Ru-N^N** was soaked in an MeCN solution (4 mL) containing $[Ru(CO)_2Cl_2]_n$ (0.5 mM) overnight. The obtained electrode was washed with MeCN and dried under dark conditions.

Fabrication of the CoO_x/$BiVO_4$ electrode

$BiVO_4$ particles were synthesized using a procedure reported elsewhere.[31,39] Briefly, the precursor oxide $K_3V_5O_{14}$ was synthesized by solid state reaction in air at 723 K for 5 h using a stoichiometric mixture of K_2CO_3 (Kanto Chemical, 99.5%) and V_2O_5 (FUJIFILM Wako Pure Chemical, 99.0%). $BiVO_4$ was then synthesized by solid–liquid reaction *via* stirring the aqueous suspension of $Bi(NO_3)_3 \cdot 6H_2O$ (Kanto Chemical, 99.9%) and $K_3V_5O_{14}$ with a stoichiometric ratio for 72 h under ambient conditions. The CoO_x cocatalyst for water oxidation was loaded by an impregnation method using a $Co(NO_3)_2$ aqueous solution, followed by calcination in air at 673 K for 2 h, with the loading amount set to 1 wt% as Co.

The photoanode for water oxidation was prepared using the CoO_x-loaded $BiVO_4$ particles using a previously reported particle transfer method.[40,41] 50 mg of the CoO_x/$BiVO_4$ powder was dispersed in 600 μL of isopropanol, and 250 μL of the suspension was dropped onto a primary glass plate (3 × 3 cm^2) and then dried in air to produce a powder layer. The Au back-contact layer was deposited on the powder layer by vacuum evaporation (Ulvac kiko, VPC-260F). The Au layer with the powder layer was bonded to an FTO with double-sided adhesive tape and lifted off the primary glass plate, and then sonicated in distilled water to remove excess particles on the particle layer. Finally, electrical contact between the Au layer and FTO was established by pure indium using a soldering iron, with unnecessary exposed parts covered with Torr Seal® (Agilent).

Photoelectrochemical measurements

An aqueous $NaHCO_3$ (50 mM) solution (15 mL) was added to a one-component electrochemical cell. The electrodes were set in the cell with an Ag/AgCl reference electrode (saturated KCl aqueous solution) and a platinum-wire counter electrode. A 300 W Xe lamp (Asahi Spectrum, MAX-302 or MAX-303) equipped with an IR-blocking mirror module was utilized as a light source. A cutoff filter (HOYA Y48 for irradiation at $\lambda_{ex} > 460$ nm or L42 for irradiation at $\lambda_{ex} > 400$ nm) or a band-pass filter (Asahi Spectra, for IPCE measurements) was employed to control the irradiation wavelength. The potential against a reversible hydrogen electrode (RHE) was calculated using the Nernst equation (eqn (1)) expressed as:

$$E(\text{V } \textit{vs.}\ \text{RHE}) = E\ (\text{V } \textit{vs.}\ \text{Ag/AgCl}) + 0.198 + 0.059\ \text{pH} \quad (1)$$

The dependence of the IPCE on the wavelength was calculated using eqn (2) expressed as:

$$\text{IPCE}\ (\%) = [(1240/\lambda_{ex})\ (I_{light} - I_{dark})/P_{light}] \times 100 \quad (2)$$

where λ_{ex} and P_{light} are the wavelength and power density of the incident light (nm and $\mu W\ cm^{-2}$), respectively, I_{light} is the current density under irradiation ($\mu A\ cm^{-2}$), and I_{dark} is the current density in the dark ($\mu A\ cm^{-2}$).

Photocatalytic CO_2 reduction using molecular photocathodes

The photoelectrochemical CO_2 reduction experiment was conducted using a Pyrex H-shaped cell with two compartments separated by a Nafion film (Aldrich, Nafion 117). The volume of each compartment was approx. 28 mL, and 15 mL of an aqueous $NaHCO_3$ (50 mM) solution was added to each compartment. The photocathode and the Ag/AgCl reference electrode were placed in the cathode compartment while the platinum-wire counter electrode was placed in the anode compartment. The three-electrode setup was used with a potentiostat (Hokuto Denko, HZ-7000) throughout the photocatalytic experiment. The experiment was conducted after purging the cathode compartment for 15 minutes using CO_2. The photocathode was irradiated at 460 nm < λ_{ex} < 650 nm using a 300 W Xe lamp (Asahi Spectrum, MAX-303) equipped with an IR-blocking mirror module with a cutoff filter (HOYA Y48). The CO and H_2 in the gas phase were analyzed with a micro-GC (Inficon, MGC3000A) and HCOOH in the solution was detected using a capillary electrophoresis apparatus (Otsuka electronics, Agilent 7100L, limit of detection is approximately 50 nmol in 15 mL of the reaction solution.).

Photocatalytic water oxidation using the photoanode

The photoelectrochemical water oxidation experiment was conducted using the setup previously described for the photocathodes. The photoanode was irradiated at 400 nm < λ_{ex} < 650 nm using a 300 W Xe lamp (Asahi Spectrum, MAX-303) equipped with an IR-blocking mirror module and a cutoff filter (HOYA L42). The amount of O_2 in the gas phase was analyzed with a micro-GC (Inficon, MGC3000A). Before the photoelectrochemical reaction, the gas phase was analyzed using the micro-GC every 5 or 15 minutes until the oxygen and nitrogen areas stabilized. Tiny amounts of gases originated from persistent air penetration, with the product amounts calculated by subtracting these as background. The nitrogen area was confirmed to be stable during the reaction, indicating that any increment in oxygen was caused by the water oxidation reaction.

Photocatalytic CO_2 reduction with water oxidation

The experiment was conducted using the setup described earlier except that a photoanode ($CoO_x/BiVO_4$) replaced the platinum-wire counter electrode. The three-electrode setup with an HZ-7000 potentiostat (Hokuto Denko) was utilized in the non-resistance ammeter mode. NiO/**PRu**-*poly*-**Ru**-**RuCAT1** (2.5 cm^2) was irradiated at 460 nm < λ_{ex} < 650 nm using a 300 W Xe lamp (Asahi Spectra MAX-303) with a cutoff filter (HOYA, Y48) and an IR-blocking mirror module. $CoO_x/BiVO_4$ (1.3 cm^2) was irradiated at 400 nm < λ_{ex} < 650 nm using a 300 W Xe lamp (Asahi Spectra MAX-302) with a cutoff filter (HOYA, L42) and an IR-blocking mirror module. The CO, H_2, HCOOH, and O_2 quantities were measured as previously described. The energy conversion efficiency (η) is calculated using eqn (3).

$$\eta(\%) = E_{chemical}/E_{photon} \times 10^2 \quad (3)$$

The chemical energy from the generated CO, HCOOH, and H_2 ($E_{chemical}$) was based on the reactions in eqn (4)–(6).

$$CO_2 \rightarrow CO + 1/2O_2\ (\Delta G^\circ = +257\ \text{kJ mol}^{-1}\text{: } \Delta E^\circ = 1.33\ \text{V}) \quad (4)$$

$$CO_2 + H_2O \rightarrow HCOOH + 1/2O_2\ (\Delta G^\circ = +270\ \text{kJ mol}^{-1}\text{: } \Delta E^\circ = 1.43\ \text{V}) \quad (5)$$

$$H_2O \rightarrow H_2 + 1/2O_2\ (\Delta G^\circ = +237\ \text{kJ mol}^{-1}\text{: } \Delta E^\circ = 1.23\ \text{V}) \quad (6)$$

The energy was then calculated using eqn (7) expressed as:

$$E_{chemical} = \Sigma[\text{Product}]2FV_{theoretical} \quad (7)$$

where [Product] is the amount of CO, HCOOH, or H_2 generated, F is the Faraday constant ($9.65 \times 10^4\ C\ mol^{-1}$), $V_{theoretical}$ is the theoretical formation voltage of each product, and E_{photon} is given by integration of the irradiated light energy ($(81\ mW\ cm^{-2} \times 2.5\ cm^2 + 61\ mW\ cm^{-2} \times 1.3\ cm^2) \times 86\ 400\ s = 24.3$ kJ).

Estimation of the amount of catalyst units on the electrode and turnover numbers for the products

By assuming that the amounts of **VRu-N^N** and Ru catalyst units are equal, the amount of Ru catalyst units on the electrode was estimated using eqn (8) expressed as:

$$n_{cat} = (n_{total} - n_{PRuV})/2 \quad (8)$$

where n_{cat}, n_{total}, and n_{PRuV} are the amount of catalyst units, the total amount of Ru complex, and the amount of **PRuV**. The n_{total} was estimated by ICP-MS and n_{PRuV} was mentioned previously. This estimation was conducted for 4 samples (Table S1†) and

the average value (37 nmol for 2.5 cm^2) was used to calculate TON in eqn (9) as:

$$\mathrm{TON} = [\mathrm{Product}]/n_{\mathrm{cat}} \quad (9)$$

where [Product] is the amount of CO, HCOOH, or H_2 generated.

Conclusions

We constructed a stable photocathode (NiO/**PRu**-*poly*-**Ru-RuCAT1**) prepared using a new stepwise approach, *i.e.*, the 1st step was adsorption of the first photosensitizer layer using methyl phosphonic acid anchor groups, the 2nd was electropolymerization of the vinyl groups for introducing additional photosensitizer units and non-coordinated bpy ligands, and the 3rd was the introduction of the catalyst units. This molecular photocathode exhibited magnificent stability and high selectivity for photoelectrochemical CO_2 reduction with high faradaic efficiency even in the aqueous solution. The turnover number of the CO_2 reduction exceeded 1200 for 100 h irradiation, with the activity of the photoelectrode maintained. Moreover, by connecting a photoanode (CoO_x/$BiVO_4$) to the photocathode, we also demonstrated durable CO_2 reduction using water as a reductant and visible light as the energy source without an external bias for 24 h, producing CO, HCOOH, and O_2 with good faradaic efficiencies.

Conflicts of interest

There are no conflicts to declare.

Acknowledgements

This work was supported by JST CREST Grant number JPMJCR13L1 in "Molecular Technology," JST Strategic International Collaborative Research Program (PhotoCAT), and JSPS KAKENHI Grant number JP17H06440 in Scientific Research on Innovative Areas "Innovations for Light-Energy Conversion." H. K. acknowledges JSPS KAKENHI Grant number JP16K21031 for Young Scientists (B). We thank Ookayama Materials Analysis Division, Technical Department from Tokyo Institute of Technology for the SEM measurement and TOF-SIMS measurement.

References

1 S. Sato, T. Arai, T. Morikawa, K. Uemura, T. M. Suzuki, H. Tanaka and T. Kajino, *J. Am. Chem. Soc.*, 2011, **133**, 15240–15243.
2 K. Sekizawa, S. Sato, T. Arai and T. Morikawa, *ACS Catal.*, 2018, **8**, 1405–1416.
3 T. M. Suzuki, S. Yoshino, T. Takayama, A. Iwase, A. Kudo and T. Morikawa, *Chem. Commun.*, 2018, **54**, 10199–10202.
4 G. Sahara, R. Abe, M. Higashi, T. Morikawa, K. Maeda, Y. Ueda and O. Ishitani, *Chem. Commun.*, 2015, **51**, 10722–10725.
5 G. Sahara, H. Kumagai, K. Maeda, N. Kaeffer, V. Artero, M. Higashi, R. Abe and O. Ishitani, *J. Am. Chem. Soc.*, 2016, **138**, 14152–14158.
6 H. Kumagai, G. Sahara, K. Maeda, M. Higashi, R. Abe and O. Ishitani, *Chem. Sci.*, 2017, **8**, 4242–4249.
7 R. Kamata, H. Kumagai, Y. Yamazaki, G. Sahara and O. Ishitani, *ACS Appl. Mater. Interfaces*, 2019, **11**, 5632–5641.
8 K. Koike, D. C. Grills, Y. Tamaki, E. Fujita, K. Okubo, Y. Yamazaki, M. Saigo, T. Mukuta, K. Onda and O. Ishitani, *Chem. Sci.*, 2018, **9**, 2961–2974.
9 Y. Yamazaki, K. Ohkubo, D. Saito, T. Yatsu, Y. Tamaki, S. i. Tanaka, K. Koike, K. Onda and O. Ishitani, *Inorg. Chem.*, 2019, **58**, 11480–11492.
10 A. Nakada, T. Nakashima, K. Sekizawa, K. Maeda and O. Ishitani, *Chem. Sci.*, 2016, **7**, 4364–4371.
11 R. Kuriki, H. Matsunaga, T. Nakashima, K. Wada, A. Yamakata, O. Ishitani and K. Maeda, *J. Am. Chem. Soc.*, 2016, **138**, 5159–5170.
12 R. Kuriki, M. Yamamoto, K. Higuchi, Y. Yamamoto, M. Akatsuka, D. Lu, S. Yagi, T. Yoshida, O. Ishitani and K. Maeda, *Angew. Chem., Int. Ed.*, 2017, **56**, 4867–4871.
13 K. Maeda, *Adv. Mater.*, 2019, **31**, e1808205.
14 T. Arai, S. Sato, K. Uemura, T. Morikawa, T. Kajino and T. Motohiro, *Chem. Commun.*, 2010, **46**, 6944–6946.
15 A. M. Lapides, D. L. Ashford, K. Hanson, D. A. Torelli, J. L. Templeton and T. J. Meyer, *J. Am. Chem. Soc.*, 2013, **135**, 15450–15458.
16 D. L. Ashford, A. M. Lapides, A. K. Vannucci, K. Hanson, D. A. Torelli, D. P. Harrison, J. L. Templeton and T. J. Meyer, *J. Am. Chem. Soc.*, 2014, **136**, 6578–6581.
17 D. L. Ashford, B. D. Sherman, R. A. Binstead, J. L. Templeton and T. J. Meyer, *Angew. Chem., Int. Ed.*, 2015, **54**, 4778–4781.
18 Y. Lattach, J. Fortage, A. Deronzier and J.-C. Moutet, *ACS Appl. Mater. Interfaces*, 2015, **7**, 4476–4480.
19 F. Li, K. Fan, L. Wang, Q. Daniel, L. Duan and L. Sun, *ACS Catal.*, 2015, **5**, 3786–3790.
20 T.-T. Li, B. Shan and T. J. Meyer, *ACS Energy Lett.*, 2019, **4**, 629–636.
21 K. Hanson, M. D. Losego, B. Kalanyan, G. N. Parsons and T. J. Meyer, *Nano Lett.*, 2013, **13**, 4802–4809.
22 K. Hanson, M. D. Losego, B. Kalanyan, D. L. Ashford, G. N. Parsons and T. J. Meyer, *Chem. Mater.*, 2013, **25**, 3–5.
23 L. Alibabaei, B. D. Sherman, M. R. Norris, M. K. Brennaman and T. J. Meyer, *Proc. Natl. Acad. Sci. U. S. A.*, 2015, **112**, 5899–5902.
24 K. L. Materna, N. Lalaoui, J. A. Laureanti, A. P. Walsh, B. P. Rimgard, R. Lomoth, A. Thapper, S. Ott, W. J. Shaw, H. Tian and L. Hammarström, *ACS Appl. Mater. Interfaces*, 2019, **12**, 4501–4509.
25 Y. Tamaki and O. Ishitani, *ACS Catal.*, 2017, **7**, 3394–3409.
26 J.-M. Lehn and R. Ziessel, *J. Organomet. Chem.*, 1990, **382**, 157–173.
27 S. Chardon-Noblat, A. Deronzier, R. Ziessel and D. Zsoldos, *Inorg. Chem.*, 1997, **36**, 5384–5389.
28 G. Balducci, E. Iengo, N. Demitri and E. Alessio, *Eur. J. Inorg. Chem.*, 2015, **2015**, 4296–4311.

29 Y. Kuramochi, J. Itabashi, K. Fukaya, A. Enomoto, M. Yoshida and H. Ishida, *Chem. Sci.*, 2015, **6**, 3063–3074.
30 Y. Yamazaki, H. Takeda and O. Ishitani, *J. Photochem. Photobiol., C*, 2015, **25**, 106–137.
31 A. Iwase, H. Ito, Q. X. Jia and A. Kudo, *Chem. Lett.*, 2016, **45**, 152–154.
32 A. Iwase, S. Ikeda and A. Kudo, *Chem. Lett.*, 2017, **46**, 651–654.
33 K. Fuku and K. Sayama, *Chem. Commun.*, 2016, **52**, 5406–5409.
34 K. Fuku, Y. Miyase, Y. Miseki, T. Funaki, T. Gunji and K. Sayama, *Chem.–Asian J.*, 2017, **12**, 1111–1119.
35 L. Tong, A. Iwase, A. Nattestad, U. Bach, M. Weidelener, G. Götz, A. Mishra, P. Bäuerle, R. Amal, G. G. Wallace and A. J. Mozer, *Energy Environ. Sci.*, 2012, **5**, 9472–9475.
36 F. Li, K. Fan, B. Xu, E. Gabrielsson, Q. Daniel, L. Li and L. Sun, *J. Am. Chem. Soc.*, 2015, **137**, 9153–9159.
37 C. D. Windle, H. Kumagai, M. Higashi, R. Brisse, S. Bold, B. Jousselme, M. Chavarot-Kerlidou, K. Maeda, R. Abe, O. Ishitani and V. Artero, *J. Am. Chem. Soc.*, 2019, **141**, 9593–9602.
38 K. Sekizawa, K. Maeda, K. Domen, K. Koike and O. Ishitani, *J. Am. Chem. Soc.*, 2013, **135**, 4596–4599.
39 A. Kudo, K. Omori and H. Kato, *J. Am. Chem. Soc.*, 1999, **121**, 11459–11467.
40 T. Minegishi, N. Nishimura, J. Kubota and K. Domen, *Chem. Sci.*, 2013, **4**, 1120–1124.
41 H. Kumagai, T. Minegishi, Y. Moriya, J. Kubota and K. Domen, *J. Phys. Chem. C*, 2014, **118**, 16386–16392.